Thermokinetic lattice Boltzmann model of nonideal fluids Supplemental Material

E. Reyhanian,[1] B. Dorschner,[1,2] and I. V. Karlin[1,*]

[1] *Department of Mechanical and Process Engineering, ETH Zurich, 8092 Zurich, Switzerland*
[2] *California Institute of Technology, Pasadena, CA 91125, USA*

(Dated: August 3, 2020)

THERMODYNAMICS

a. Internal energy To capture the correct thermodynamics of the real gas, it is essential to use the correct thermodynamical relations. Real gases differ from ideal gas in the sense that the internal energy and enthalpy are no longer the function of temperature only. Instead, they depend on two thermodynamical parameters namely, $e = e(T, v)$ and $h = h(T, p)$ where v is the specific volume of the fluid. Therefore the internal energy of a real gas can be described as

$$de = C_v dT + \left(\frac{\partial e}{\partial v}\right)_T dv \tag{1}$$

Where C_v is the specific heat at constant volume which is considered as constant in the "polytropic" assumption [1–3]. To compute the non-tangible part of Eq. (1), the well-known thermodynamical relation $Tds = de + pdv$ is put to use

$$T\left(\frac{\partial s}{\partial v}\right)_T = \left(\frac{\partial e}{\partial v}\right)_T + p \tag{2}$$

Using the famous Maxwell relation $\left(\frac{\partial s}{\partial v}\right)_T = \left(\frac{\partial p}{\partial T}\right)_v$ leads to the differential equation for real gas internal energy

$$de = C_v dT + \left[T\left(\frac{\partial p}{\partial T}\right)_v - p\right] dv \tag{3}$$

b. Calculation of C_p Specific heat capacity at constant pressure is defined as

$$C_p = \left(\frac{\partial h}{\partial T}\right)_p = \left(\frac{\partial e}{\partial T}\right)_p + p\left(\frac{\partial v}{\partial T}\right)_p \tag{4}$$

where the expression of enthalpy $h = e + pv$ is used. According to Eq. (3) one can write

$$\left(\frac{\partial e}{\partial T}\right)_p = C_v + \left[T\left(\frac{\partial p}{\partial T}\right)_v - p\right]\left(\frac{\partial v}{\partial T}\right)_p \tag{5}$$

Finally, the expression for the C_p of a real-gas is obtained as

$$C_p = C_v + T\left(\frac{\partial p}{\partial T}\right)_v \left(\frac{\partial v}{\partial T}\right)_p \tag{6}$$

c. Speed of sound The theoretical description of speed of sound in a real-gas originates from its definition

$$\varsigma^2 = \left(\frac{\partial p}{\partial \rho}\right)_s = -v^2\left(\frac{\partial p}{\partial v}\right)_s \tag{7}$$

Using the well-known cyclic relation, we obtain

$$\left(\frac{\partial p}{\partial v}\right)_s = -\left(\frac{\partial p}{\partial s}\right)_v \div \left(\frac{\partial v}{\partial s}\right)_p \tag{8}$$

The terms on the R.H.S of Eq. (8) can be substituted by their counterparts using the Maxwell relations

$$-\left(\frac{\partial p}{\partial s}\right)_v = \left(\frac{\partial T}{\partial v}\right)_s \tag{9}$$

$$\left(\frac{\partial v}{\partial s}\right)_p = \left(\frac{\partial T}{\partial p}\right)_s \tag{10}$$

Applying the cyclic relation to the R.H.S of Eqs. (9) and (10) leads to

$$-\left(\frac{\partial T}{\partial v}\right)_s = \frac{T}{C_v}\left(\frac{\partial p}{\partial T}\right)_v \tag{11}$$

$$\left(\frac{\partial T}{\partial p}\right)_s = \frac{T}{C_p}\left(\frac{\partial v}{\partial T}\right)_p \tag{12}$$

Finally the expression for speed of sound is obtained as

$$\varsigma^2 = \frac{C_p}{C_v}\left(\frac{\partial p}{\partial \rho}\right)_T \tag{13}$$

By using Eq. (6), we get the following thermodynamical relation for speed of sound in a real gas medium

$$\varsigma = \sqrt{\left(\frac{\partial p}{\partial \rho}\right)_T + \frac{T}{\rho^2 c_v}\left(\frac{\partial p}{\partial T}\right)_\rho^2} \tag{14}$$

Which implies that the isentropic speed of sound is always higher than that in isothermal condition. For the van der Waals EoS, one can simply derive the following expressions,

$$e_{vdw} = C_v T - a\rho, \tag{15}$$

$$C_{p_{vdw}} = C_v + \frac{R^2 T}{RT - 2a\rho(1-b\rho)^2}, \tag{16}$$

$$\varsigma_{vdw} = \sqrt{\frac{RT}{(1-b\rho)^2}(1+\delta) - 2a\rho}, \tag{17}$$

* Corresponding author; karlin@lav.mavt.ethz.ch

EQUILIBRIUM

We consider the standard nine-velocity model, the *D2Q9* lattice. The discrete speeds are constructed as atensor product of two one-dimensional peculiar speeds, $c_i = i$, where $i = 0, \pm 1$. Discrete speeds in two-dimensions are

$$\mathbf{c}_{(i,j)} = (c_i, c_j)^\dagger, \tag{18}$$

where we have introduced two-dimensional indices in order to reflect the Cartesian frame instead of a more common single subscript. Thus, the discrete velocities are defined as

$$\mathbf{v}_{(i,j)} = \sqrt{\theta}(c_i, c_j)^\dagger + (u_x, u_y)^\dagger \tag{19}$$

with reduced temperature $\theta = p/(\rho T_L)$ and lattice temperature $T_L = 1/3$. Populations are labeled with two indices, $f_{(i,j)}$, corresponding to their respective velocities (19). The local equilibrium populations are now conveniently expressed as the product of one-dimensional weights

$$f^{eq}_{(i,j)} = \rho W_{(i,j)} = \rho W_i W_j \tag{20}$$

Where

$$W_i = \begin{cases} 2/3, \text{ for i=0} \\ 1/6, \text{ otherwise} \end{cases} \tag{21}$$

While the equilibrium populations are constant up to the proportionality to density, their moments

$$M^{eq}_{mn} = \rho \sum_{(i,j)} W_i W_j (\sqrt{\theta} c_i + u_x)^m (\sqrt{\theta} c_j + u_y)^n, \tag{22}$$

recover the pertinent nine Maxwell-Boltzmann moments up to the fourth order, $0 \leqslant m \leqslant 2$, $0 \leqslant n \leqslant 2$, $m+n \leqslant 4$, without error for any velocity.

TRANSFER MATRIX

Populations $f^\lambda_{(i,j)}$ measured in the gauge λ, can be represented as linear combinations of nine linearly independent moments,

$$M^\lambda = (M^\lambda_{00}, M^\lambda_{10}, M^\lambda_{01}, M^\lambda_{11}, M^\lambda_{20}, M^\lambda_{02}, M^\lambda_{21}, M^\lambda_{12}, M^\lambda_{22})^\dagger \tag{23}$$

Where

$$M_{mn} = \sum_{(i,j)} f^\lambda_{(i,j)} (\sqrt{\theta} c_i + u_x)^m (\sqrt{\theta} c_j + u_y)^n, \tag{24}$$

and $\mathcal{M}^\lambda$ is the $Q \times Q$ matrix of the linear map between populations and moments,

$$\mathcal{M}_\lambda f^\lambda = M^\lambda \tag{25}$$

Moments are invariant with respect to the gauge,

$$\mathcal{M}_{\lambda'} f^{\lambda'} = \mathcal{M}_\lambda f^\lambda \tag{26}$$

This implies that the populations are transformed from one gauge to another with the transfer matrix $\mathcal{G}^{\lambda'}_\lambda$,

$$f^{\lambda'} = \mathcal{G}^{\lambda'}_\lambda f^\lambda = \mathcal{M}^{-1}_{\lambda'} \mathcal{M}_\lambda f^\lambda \tag{27}$$

The transfer from gauge λ to λ' can also be written in the following explicit form,

$$f^{\lambda'}_{kl} = w(k) w(l) \sum_{(i,j)} g_x(i,k) g_y(j,l) f^\lambda_{(i,j)}, \tag{28}$$

Where

$$g_\xi(i,j) = A^2_\xi(i) - B_\xi(i,j), \tag{29}$$

$$A_\xi(i) = \left(u'_\xi - u_\xi\right)/\sqrt{3} - i\sqrt{p/\rho}, \tag{30}$$

$$B_\xi(i,j) = \begin{cases} p'/\rho', & \text{for j=0,} \\ j\sqrt{p'/\rho'} A_\xi(i), & \text{otherwise,} \end{cases} \tag{31}$$

$$w(i) = \begin{cases} 1/(\frac{p'}{\rho'}), & \text{for i=0,} \\ -1/2(\frac{p'}{\rho'}), & \text{otherwise.} \end{cases} \tag{32}$$

Formula (28) only involves evaluation of a dot-product as opposed to numerically solving the linear system (26).

RECONSTRUCTION

An equidistant rectilinear mesh with $\Delta x = 1$ is used for all simulations. Populations at off-grid locations are reconstructed using 3^{rd}-order polynomial interpolation,

$$\tilde{f}^\lambda_{(i,j)}(\boldsymbol{x}, t) = \sum_{\substack{0 \leq m \leq 3 \\ 0 \leq n \leq 3}} a_{mn}(\boldsymbol{x})\, f^\lambda_{(i,j)}((x_0 + n, y_0 + m), t), \tag{33}$$

where the populations at integer collocation points $(x_0 + n, y_0 + m)$ are transformed to gauge λ using Eq. (28) and a_{mn} are standard Lagrange polynomials,

$$a_{mn}(\boldsymbol{x}) = \prod_{\substack{0 \leq k \leq 3 \\ k \neq n}} \frac{(x - x_0) - k}{n - k} \prod_{\substack{0 \leq l \leq 3 \\ l \neq m}} \frac{(y - y_0) - l}{m - l}, \tag{34}$$

with respect to reference coordinate,

$$\boldsymbol{x}_0 = (\lfloor x \rfloor - 1, \lfloor y \rfloor - 1), \tag{35}$$

where the operation $\lfloor \phi \rfloor$ rounds down to the largest integer value not greater than ϕ.

SPEED OF SOUND

First, we consider the simplified EOS near the critical point, where the free-energy takes the following form [4]

$$E_0 = \beta(\rho - \rho^{sat}_l)(\rho - \rho^{sat}_v), \tag{36}$$

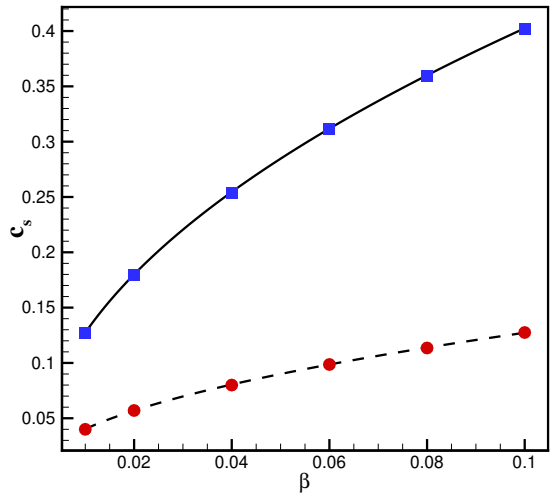

FIG. 1. Speed of sound in a simplified EOS near the critical point. line: liquid (theory), dashed: vapor (theory), symbols: present. Values of speed of sound are preseted in lattice units.

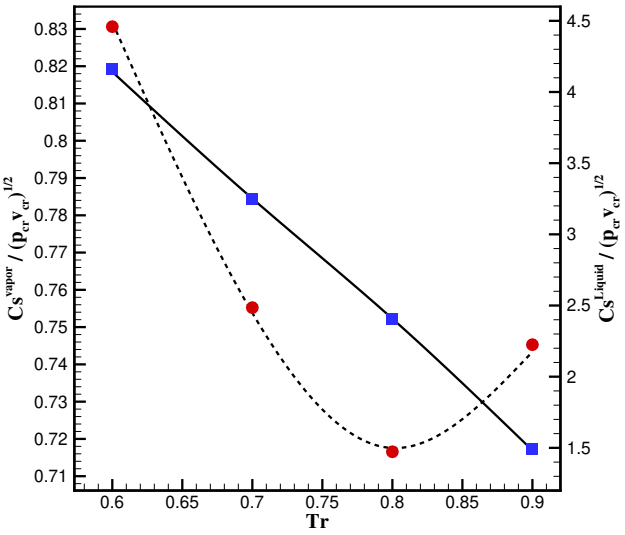

FIG. 2. Isothermal speed of sound in a van der Waals fluid. line: liquid (theory), dashed: vapor (theory), symbols: present.

where β is a function of temperature and ${\rho_l}^{sat}$ and ${\rho_v}^{sat}$ are the saturated densities of the liquid and vapor phase, respectively [4]. The thermodynamic pressure can now be obtained as $p = \rho\partial E_0/\partial\rho - E_0$. In this special case, the isentropic speed of sound coincides with the isothermal one since the partial derivation of pressure to temperature at saturated liquid and vapor densities is simply zero. Hence, the speed of sound in the simplified EOS at saturated conditions reads

$$\varsigma|_{\rho_l^{sat}} = (\rho_l^{sat} - \rho_v^{sat})\sqrt{2\beta\rho_l^{sat}}, \tag{37}$$

$$\varsigma|_{\rho_v^{sat}} = (\rho_l^{sat} - \rho_v^{sat})\sqrt{2\beta\rho_v^{sat}}, \tag{38}$$

choosing the density ratio as $\rho_l/\rho_v = 10$, the measured value of speed of sound in the simulations are compared with theoretical expressions in Fig.1. The results for both liquid and gas phases show excellent agreement.
The isothermal simulation is repeated with the same setup for the van der Waals fluid and Fig. 2 shows excellent agreement between theory and simulation.

COEXISTENCE CURVE

In this part, isothermal simulation of the coexistence curve is conducted with the Dieterici EOS

$$p = \frac{\rho RT}{1 - b\rho} exp(-\frac{a\rho}{RT}) \tag{39}$$

Introducing the critical properties as $\rho_{cr} = 1/(2b)$, $T_{cr} = a/(4Rb)$ and $p_{cr} = a/(2eb)^2$ [5], the reduced form of this EOS reads

$$p_r = \frac{\rho_r T_r e^2}{2 - \rho_r} exp\left(-\frac{2\rho_r}{T_r}\right) \tag{40}$$

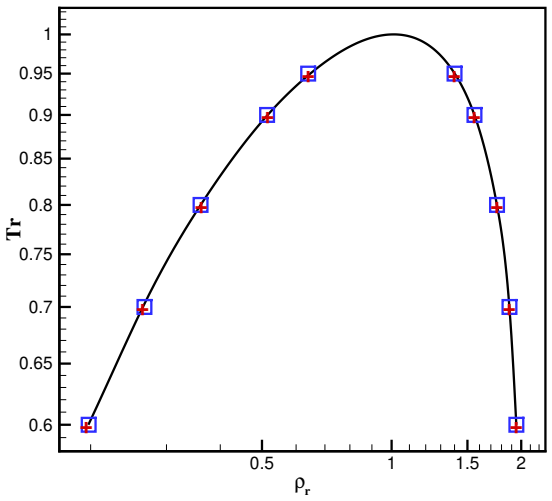

FIG. 3. Isothermal simulation of the coexistence curve employing the Dietrici EOS. line: Maxwell, square: Present, cross: LBM.

where the reduced quantities are scaled to their corresponding critical values. Note that here $e = exp(1)$ is the Euler's number and it shall not be confused with internal energy. Simulation results are illustrated in Fig. 3 and compared to predicted values by Maxwell construction.

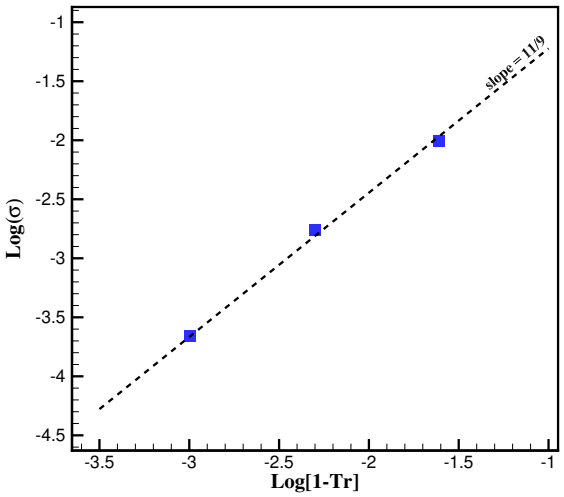

FIG. 4. Temperature dependency of surface tension. square: present, dashed: empirical slope predicted by Eq. (41)

SURFACE TENSION

Continuing with the Dieterici EOS, the temperature dependency of the surface tension is evaluated. Surface tension of a liquid is a decreasing function of temperature and it vanishes when the system approaches the critical point. According to the Guggenheim−Katayama relation, this behavior can be formulated by [6]

$$\sigma = \sigma_0 (1 - T_r)^{11/9} \tag{41}$$

Where σ_0 is a constant. The values of the surface tension is obtained by the Laplace law at each temperature simulating a 2D droplet. Fig. 4 shows that there is good agreement between simulation results and predicted values by Eq. (41).

RANKINE-HUGONIOT CONDITIONS

The shock front traveling with speed s separates the domain into two parts; Ω_1 the post-shock part and Ω_0 the pre-shock part. Shock waves must satisfy the Rankine-Hugoniot relations

$$-s\langle M\rangle + \langle N\rangle = 0, \tag{42}$$
$$M = \begin{bmatrix} \rho \\ \rho u \\ \rho E \end{bmatrix}, \; N = \begin{bmatrix} \rho u \\ p + \rho u^2 \\ \rho u H \end{bmatrix},$$

where the operator $\langle\phi\rangle = \phi_1 - \phi_0$ represents the jump of the quantity ϕ across the shock front. Assuming the shock front propagates in a still enviroment ($u_0 = 0$) and by taking the density of the post-shock region, i.e., ρ_1, as the free parameter, the post-shock properties for the van der Waals fluid in terms of non-dimensional quantities are obtained as [1]

$$M_0 = \frac{1}{\tilde{c}_{s0}} \sqrt{6\tilde{\rho}_1 \frac{\tilde{p}_0(1+\delta) + \tilde{\rho}_0\tilde{\rho}_1(\tilde{\rho}_0 + \tilde{\rho}_1 + 3\delta - 3)}{\tilde{\rho}_0(2\tilde{\rho}_0(3 - \tilde{\rho}_1) + 3\delta(\tilde{\rho}_0 - \tilde{\rho}_1))}} \tag{43}$$

$$\tilde{u}_1 = \tilde{\varsigma}_1 M_0 \frac{\tilde{\rho}_1 - \tilde{\rho}_0}{\tilde{\rho}_1} \tag{44}$$

$$\tilde{p}_1 = \tilde{p}_0 + \tilde{\varsigma}_0^2 M_0^2 \frac{\tilde{\rho}_0(\tilde{\rho}_1 - \tilde{\rho}_0)}{\tilde{\rho}_1} \tag{45}$$

where $(\tilde{u}, \tilde{\varsigma}) = (u, \varsigma)/\sqrt{p_{cr} v_{cr}}$, $\tilde{p} = p/p_{cr}$ and $\tilde{\rho} = \rho/\rho_{cr}$.

SHOCK TUBE

For $\delta \leqslant \delta_{BZT} = 0.06$ there exists a region near the saturated vapor, where non-classical behavior may be observed [1, 2]. As mentioned in the main text, this can be characterized by the so called fundamental derivative Γ. Following the definition of Γ and considering the van der Waals fluid, one can derive

$$\Gamma(p, v) = \frac{(\delta+1)(\delta+2)\frac{p + a/v^2}{(v-b)^2} - \frac{6a}{v^4}}{2(\delta+1)\frac{p + a/v^2}{v(v-b)} - \frac{4a}{v^4}} \tag{46}$$

Depending on the sign of Γ and whether the $\Gamma = 0$ line is crossed during the evolution of the fluid or not, different outcomes may appear [7]. According to Ref. [2] two more shock-tube cases are considered here to assess the range of validity of the scheme. The conditions on the left and right sides of the shock tube toghether with the value of δ corresponding to each case are listed in Table I. The shock front is initially located on the half-length of the tube. The results for both cases are illustrated in Fig. 5 and Fig. 6 at different times. As expected, no anomalous behavior is observed in the first case since $\delta = 0.329 > \delta_{BZT}$. The pressure and density field shows a classic compression shock traveling towards the right side of the tube accompanied by a rarefaction wave moving to the opposite side. The second case however, is different in terms of existence of non-classical region near the saturation vapor line in the $p - v$ diagram. Although the values of Γ for both the left and right parts of the tube is positive, the $\Gamma = 0$ line is crossed during the evolution of the flow. This change of sign results in the mixed rarefaction wave composed of a rarefaction shock connected to a rarefaction fan. Meanwhile, a compression shock is traveling toward the low pressure side. The

TABLE I. Shock tube conditions

Case	(p_L, ρ_L)	(p_R, ρ_R)	(Γ_L, Γ_R)	δ
I	(1.6077,1.01)	(0.8957,0.594)	(2.239,1.361)	0.329
II	(3.00,1.818)	(0.575,0.275)	(4.118,0.703)	0.0125

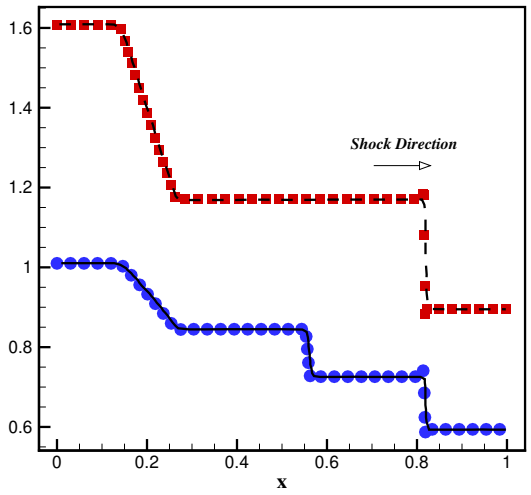

FIG. 5. Simulation of shock-tube problem case I at $t^* = 0.2$. Line: density [2]. Dashed: pressure [2]. Symbols: present

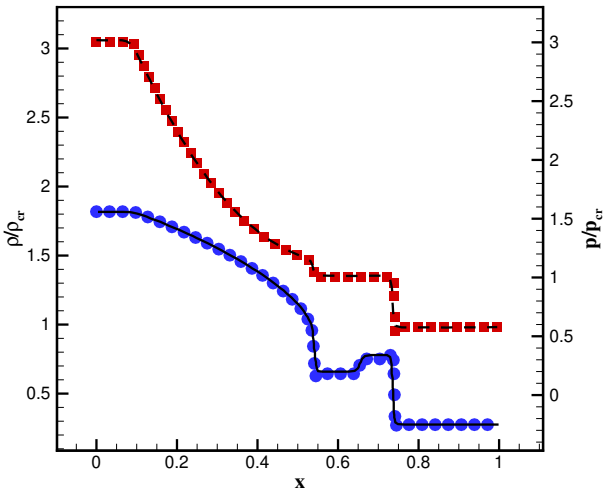

FIG. 6. Simulation of shock-tube problem case II at $t^* = 0.15$. Line: density [2]. Dashed: pressure [2]. Symbols: present

latter case together with the studied item in the main text compose the typical examples of "non-classical gas dynamics", where we can observe anomalous phenomena such as rarefaction shock waves and mixed rarefaction waves. The results show that the present scheme have successfully recovered the non-classic dynamics of a real gas.

CHAPMAN-ENSKOG EXPANSION

Here we aim at recovering the macroscopic Navier-Stokes equations from the dynamics of kinetic equations (3-6) in the main text. To this end, the pertinent equilibrium moments of f and g populations are required, which are computed as follows:

$$P^{eq}_{\alpha\beta} = \sum_{i=0}^{Q} f_i^{eq} v_{i\alpha} v_{i\beta} = \rho u_\alpha u_\beta + p\delta_{\alpha\beta}, \tag{47}$$

$$Q^{eq}_{\alpha\beta\gamma} = \sum_{i=0}^{Q} f_i^{eq} v_{i\alpha} v_{i\beta} v_{i\gamma} = \rho u_\alpha u_\beta u_\gamma + p[u\delta]_{\alpha\beta\gamma}, \tag{48}$$

$$q^{eq}_{\alpha} = \sum_{i=0}^{Q} g_i^{eq} v_{i\alpha} = 2\rho u_\alpha H, \tag{49}$$

$$R^{eq}_{\alpha\beta} = \sum_{i=0}^{Q} g_i^{eq} v_{i\alpha} v_{i\beta} = 2\rho u_\alpha u_\beta \left(H + p/\rho\right) + 2pH\delta_{\alpha\beta}, \tag{50}$$

where $[u\delta]_{\alpha\beta\gamma} = u_\alpha\delta_{\beta\gamma} + u_\beta\delta_{\alpha\gamma} + u_\gamma\delta_{\alpha\beta}$ and H is the total enthalpy. Note that equations (49) and (50) are the desired moments, which the equilibrium g_i^{eq} is constructed upon them. First, we introduce the following expansions:

$$f_i = f_i^{(0)} + \epsilon f_i^{(1)} + \epsilon^2 f_i^{(2)}, \tag{51}$$

$$g_i = g_i^{(0)} + \epsilon g_i^{(1)} + \epsilon^2 g_i^{(2)}, \tag{52}$$

$$\partial_t = \epsilon\partial_t^{(1)} + \epsilon^2\partial_t^{(2)}, \tag{53}$$

$$\partial_\alpha = \epsilon\partial_\alpha^{(1)}. \tag{54}$$

Applying the Taylor expansion up to second order and separating the orders of ϵ results in:

$$\{f_i^{(0)}, g_i^{(0)}\} = \{f_i^{eq}, g_i^{eq}\}, \tag{55}$$

$$\partial_t^{(1)}\{f_i^{(0)}, g_i^{(0)}\} + v_{i\alpha}\partial_\alpha^{(1)}\{f_i^{(0)}, g_i^{(0)}\} = -(\omega/\delta t)\{f_i^{(1)}, g_i^{(1)}\}, \tag{56}$$

$$\partial_t^{(2)}\{f_i^{(0)}, g_i^{(0)}\} + \left(\partial_t^{(1)} + v_{i\alpha}\partial_\alpha^{(1)}\right)(1 - \frac{\omega}{2})\{f_i^{(1)}, g_i^{(1)}\} = -(\omega/\delta t)\{f_i^{(2)}, g_i^{(2)}\}. \tag{57}$$

The local conservation of density, momentum and energy imply

$$\sum_{i=0}^{Q}\{f_i^{(n)}, g_i^{(n)}\} = 0, n \geq 1, \tag{58}$$

$$\sum_{i=0}^{Q} f_i^{(n)} v_{i\alpha} = 0, n \geq 1 \tag{59}$$

Applying conditions (58) and (59) on equation (56), we derive the following first order equations,

$$D_t^{(1)}\rho = -\rho\partial_\alpha^{(1)}u_\alpha, \tag{60}$$

$$D_t^{(1)}u_\alpha = -\frac{1}{\rho}\partial_\alpha^{(1)}p, \tag{61}$$

$$D_t^{(1)}T = -\frac{T}{\rho C_v}\left(\frac{\partial p}{\partial T}\right)_\rho \partial_\alpha^{(1)}u_\alpha, \tag{62}$$

where $D_t^{(1)} = \partial_t^{(1)} + u_\alpha\partial_\alpha^{(1)}$ is the first order total-derivative. Note that, the thermodynamic relations (1-15) together with equations (60) and (61) have been used in deriving the first-order temperature equation (62). Subsequently, we can derive a similar equation for pressure considering that $p = p(\rho, T)$. This yields

$$D_t^{(1)}p = \left(\frac{\partial p}{\partial \rho}\right)_T D_t^{(1)}\rho + \left(\frac{\partial p}{\partial T}\right)_\rho D_t^{(1)}T = -\rho\varsigma^2\partial_\alpha^{(1)}u_\alpha, \tag{63}$$

where ς^2 is given by equation (14).
The second order relations are obtained by applying the conditions (58) and (59) on equation (57),

$$\partial_t^{(2)}\rho = 0, \tag{64}$$

$$\partial_t^{(2)}u_\alpha = \frac{1}{\rho}\partial_\beta^{(1)}\left[\delta t\left(\frac{1}{\omega}-\frac{1}{2}\right)\left(\partial_t^{(1)}P^{eq}_{\alpha\beta} + \partial_\gamma^{(1)}Q^{eq}_{\alpha\beta\gamma}\right)\right], \tag{65}$$

$$\partial_t^{(2)}T = \frac{1}{2\rho C_v}\left\{\partial_\alpha^{(1)}\left[\delta t\left(\frac{1}{\omega}-\frac{1}{2}\right)\left(\partial_t^{(1)}q_\alpha^{eq} + \partial_\beta^{(1)}R^{eq}_{\alpha\beta}\right)\right] - 2\rho u_\alpha\partial_t^{(2)}u_\alpha\right\}. \tag{66}$$

Equations (60) and (64) constitute the continuity equation. The non-equilibrium pressure tensor and heat flux in the R.H.S of equations (65) and (66) are evaluated using equations (60-63),

$$\begin{aligned}\partial_t^{(1)}P^{eq}_{\alpha\beta} + \partial_\gamma^{(1)}Q^{eq}_{\alpha\beta\gamma} = {}& p\left(\partial_\beta^{(1)}u_\alpha + \partial_\alpha^{(1)}u_\beta\right)\\ &+ \left(p-\rho\varsigma^2\right)\partial_\gamma^{(1)}u_\gamma\delta_{\alpha\beta}\end{aligned} \tag{67}$$

$$\begin{aligned}\partial_t^{(1)}q_\alpha^{eq} + \partial_\beta^{(1)}R^{eq}_{\alpha\beta} = {}& 2\left(p-\rho\varsigma^2\right)\partial_\gamma^{(1)}u_\gamma u_\alpha\\ &+ 2pu_\beta\left(\partial_\beta^{(1)}u_\alpha + \partial_\alpha^{(1)}u_\beta\right) + 2p\partial_\alpha^{(1)}h\end{aligned} \tag{68}$$

where $h = e + p/\rho$ is the specific enthalpy. Finally, summing up the contributions of density, momentum and temperature at the ϵ and ϵ^2 orders, we get the hydrodynamic limit of the model, which reads

$$D_t\rho = -\rho\nabla\cdot\boldsymbol{u}, \tag{69}$$

$$\rho D_t\boldsymbol{u} = -\nabla p - \nabla\cdot\boldsymbol{\tau}, \tag{70}$$

$$\rho C_v D_t T = -\boldsymbol{\tau}:\nabla\boldsymbol{u} - T\left(\frac{\partial p}{\partial T}\right)_v \nabla\cdot\boldsymbol{u} - \nabla\cdot\boldsymbol{q}, \tag{71}$$

We must comment that the expression of heat flux recovered from the Chapman-Enskog analysis without the correction term in the g population is found as $\boldsymbol{q}^{\mathrm{CE}} = -\mu\nabla h$. At the limit of an ideal-gas, this is equivalent to the fourier law $\boldsymbol{q}_{\mathrm{ig}} = -k_{\mathrm{ig}}\nabla T$ where $k_{\mathrm{ig}} = \mu C_p^{\mathrm{ig}}$ and hence the Prandtl number is fixed to $\mathrm{Pr} = \mu C_p^{\mathrm{ig}}/k_{\mathrm{ig}} = 1$ due to the single relaxation time BGK collision model. However, considering the enthalpy of a real-gas as function of pressure and temperature, we have, $\nabla h = C_p\nabla T + v(1-\beta T)\nabla p$, where $v = 1/\rho$ is the specific volume, $\beta = v^{-1}\left(\partial v/\partial T\right)_p$ is the thermal expansion coefficient and $C_p = C_v + Tv\beta\left(\partial p/\partial T\right)_v$ is the specific heat at constant pressure. While one could eliminate the pressure part of the enthalpy by the correction term and only retain the temperature dependent part, it must be noted that the thermal expansion coefficient *at* the critical point diverges, $\beta\to\infty$ and so does the specific heat $C_p\to\infty$. Hence to recover the well-known Fourier law, the post-collision of the g population is augmented by the correction term $G_i\delta t$ where $\sum G_i = -2\nabla\cdot(\mu\nabla h) + 2\nabla\cdot(k\nabla T)$ with all the other moments equal to zero. We can take such a population as,

$$G_i = M_0 W_i\left(1 + \frac{\rho(\boldsymbol{u}\cdot\boldsymbol{c}_i)^2}{2pT_{\mathrm{L}}} - \frac{\rho v_i^2}{2p} + \frac{D}{2}\right), \tag{72}$$

where $M_0 = \sum G_i$. A similar anomaly in the expression for the heat flux was observed and reported in [8].

Including the force

As mentioned in the main text, the force terms in the kinetic equations represent the interface dynamics. First, we recast the post-collision state of the f population in the following form [9],

$$f_i^*(\boldsymbol{x},t) = f_i(\boldsymbol{x},t) + \omega(f_i^{eq}(\rho,\hat{\boldsymbol{u}}) - f_i(\boldsymbol{x},t)) + \hat{S}_i, \tag{73}$$

$$\hat{\boldsymbol{u}} = \boldsymbol{u} + \frac{\boldsymbol{F}\delta t}{2\rho}, \tag{74}$$

$$\hat{S}_i = S_i - \omega\left(f_i^{eq}(\rho,\hat{\boldsymbol{u}}) - \rho W_i\right), \tag{75}$$

where $[S_i = f_i^{eq}(\rho, \boldsymbol{u} + \boldsymbol{F}\delta t/\rho) - \rho W_i]$ and $\boldsymbol{F} = -\nabla\cdot\boldsymbol{K}$. Here we expand the forcing term $\hat{S}_i^{(1)} = \epsilon\hat{S}_i^{(1)}$ in addition to the expansions (51,53,54). Similarly, we get the following relations at the orders of $\epsilon^0, \epsilon^1, \epsilon^2$ respectively,

$$f_i^{(0)} = f_i^{eq}(\rho,\hat{\boldsymbol{u}}), \tag{76}$$

$$\partial_t^{(1)}f_i^{(0)} + v_{i\alpha}\partial_\alpha^{(1)}f_i^{(0)} = -(\omega/\delta t)f_i^{(1)} + \frac{1}{\delta t}\hat{S}_i^{(1)}, \tag{77}$$

$$\partial_t^{(2)}f_i^{(0)} + \left(\partial_t^{(1)} + v_{i\alpha}\partial_\alpha^{(1)}\right)(1-\frac{\omega}{2})f_i^{(1)} + \frac{1}{2}\left(\partial_t^{(1)} + v_{i\alpha}\partial_\alpha^{(1)}\right)\hat{S}_i^{(1)} = -(\omega/\delta t)f_i^{(2)}, \tag{78}$$

It is important here to assess the solvability conditions imposed by the local conservations. Considering the

moment-invariant property of the transfer matrix between the two gauges $\boldsymbol{u}$ and $\hat{\boldsymbol{u}}$, one can easily compute,

$$\sum_{i=0}^{Q} f_i^{(0)} = \sum_{i=0}^{Q} f_i^{eq}(\rho, \hat{\boldsymbol{u}}) = \rho, \tag{79}$$

$$\sum_{i=0}^{Q} f_i^{(0)} v_{i\alpha} = \sum_{i=0}^{Q} f_i^{eq}(\rho, \hat{\boldsymbol{u}}) v_{i\alpha} = \rho \hat{u}_\alpha. \tag{80}$$

This implies that,

$$\sum_{i=0}^{Q} f_i^{(n)} = 0, n \geq 1, \tag{81}$$

$$\sum_{i=0}^{Q} f_i^{(n)} v_{i\alpha} = \begin{cases} -\frac{\delta t}{2} F_\alpha^{(1)} & \text{,n=1} \\ 0 & \text{,n>1} \end{cases} \tag{82}$$

According to the definition of S_i, the following moments can be computed:

$$\sum_{i=0}^{Q} \hat{S}_i^{(1)} = 0, \tag{83}$$

$$\sum_{i=0}^{Q} \hat{S}_i^{(1)} v_{i\alpha} = \delta t (1 - \frac{\omega}{2}) F_\alpha^{(1)}, \tag{84}$$

$$\sum_{i=0}^{Q} \hat{S}_i^{(1)} v_{i\alpha} v_{i\beta} = \delta t (1 - \frac{\omega}{2}) \left(\hat{u}_\alpha F_\beta + \hat{u}_\beta F_\alpha\right) + \frac{\omega \delta t^2 F_\alpha F_\beta}{4\rho}. \tag{85}$$

Similarly, the first order equations of density and momentum are derived by applying the solvability conditions (81) and (82) on equations (77) and (78),

$$\hat{D}_t^{(1)} \rho = -\rho \partial_\alpha^{(1)} \hat{u}_\alpha, \tag{86}$$

$$\hat{D}_t^{(1)} \hat{u}_\alpha = -\frac{1}{\rho} \partial_\alpha^{(1)} p + \frac{1}{\rho} F_\alpha^{(1)}, \tag{87}$$

where $\hat{D}_t^{(1)} = \partial_t^{(1)} + \hat{u}_\alpha \partial_\alpha^{(1)}$. At this point it is necessary to mention that since there is a force added to the momentum equation (in this case the divergence of the Korteweg stress), it should also be considered in the energy equation as well. Hence, M_0 in Eq. (72) is modified to,

$$M_0 = -2\nabla \cdot (\mu \nabla h) + 2\nabla \cdot (k \nabla T) + 2\hat{u}_\alpha F_\alpha, \tag{88}$$

The equilibrium moments are modified as,

$$\sum_{i=0}^{Q} g_i^{eq} = 2\rho \hat{E}, \tag{89}$$

$$q_\alpha^{eq} = \sum_{i=0}^{Q} g_i^{eq} v_{i\alpha} = 2\rho \hat{u}_\alpha \hat{H}, \tag{90}$$

$$R_{\alpha\beta}^{eq} = \sum_{i=0}^{Q} g_i^{eq} v_{i\alpha} v_{i\beta} = 2\rho \hat{u}_\alpha \hat{u}_\beta \left(\hat{H} + p/\rho\right) + 2p\hat{H}\delta_{\alpha\beta}, \tag{91}$$

where $\hat{E} = e + \hat{u}^2/2$ and $\hat{H} = \hat{E} + p/\rho$. With the changes mentioned so far, the first-order equation of temperature is derived as

$$\hat{D}_t^{(1)} T = -\frac{T}{\rho C_v} \left(\frac{\partial p}{\partial T}\right)_\rho \partial_\alpha^{(1)} \hat{u}_\alpha. \tag{92}$$

Finally, in a similar manner as the case without the force the macroscopic equations are recovered by collecting the equations of density, momentum and temperature at each order,

$$\hat{D}_t \rho = -\rho \nabla \cdot \hat{\boldsymbol{u}}, \tag{93}$$

$$\rho \hat{D}_t \boldsymbol{u} = -\nabla p - \nabla \cdot \hat{\boldsymbol{\tau}} - \nabla \cdot \boldsymbol{K}, \tag{94}$$

$$\rho C_v \hat{D}_t T = -\hat{\boldsymbol{\tau}} : \nabla \hat{\boldsymbol{u}} - T \left(\frac{\partial p}{\partial T}\right)_v \nabla \cdot \hat{\boldsymbol{u}} - \nabla \cdot \boldsymbol{q}, \tag{95}$$

$$\hat{\boldsymbol{\tau}} = -\mu \left(\nabla \hat{\boldsymbol{u}} + \nabla \hat{\boldsymbol{u}}^\dagger - \frac{2}{D} (\nabla \cdot \hat{\boldsymbol{u}}) \boldsymbol{I}\right) - \eta (\nabla \cdot \hat{\boldsymbol{u}}) \boldsymbol{I}, \tag{96}$$

It should be noted that the error terms associated with the forcing are not shown here. For instance, as reported in the literature [9–11] one can show that the error term in the momentum equation appears as $\nabla \cdot (\delta t^2 \boldsymbol{F}\boldsymbol{F}/4\rho)$.

The total energy of the fluid is formulated by $\hat{\mathcal{E}} = e(T, v) + \hat{u}^2/2 + E_\lambda$ where $E_\lambda = \kappa |\nabla \rho|^2/2$ is the non-local part corresponding to the excess energy of the interface. The evolution equation for the specific internal energy $e(T, v)$ can be obtained by considering equations (3,93,95)

$$\rho \hat{D}_t e = -p \nabla \cdot \hat{\boldsymbol{u}} - \hat{\boldsymbol{\tau}} : \nabla \hat{\boldsymbol{u}} - \nabla \cdot \boldsymbol{q}, \tag{97}$$

From the momentum equation (94) we get,

$$\frac{1}{2} \rho \hat{D}_t \hat{u}^2 = -\hat{\boldsymbol{u}} \cdot \nabla p - \hat{\boldsymbol{u}} \cdot \nabla \cdot \hat{\boldsymbol{\tau}} - \hat{\boldsymbol{u}} \cdot \nabla \cdot \boldsymbol{K}, \tag{98}$$

and the evolution of the excess energy can be computed using the continuity equation,

$$\rho \hat{D}_t E_\lambda = -\boldsymbol{K} : \nabla \hat{\boldsymbol{u}} - \nabla \cdot \left(\kappa \rho \nabla \cdot \hat{\boldsymbol{u}} \nabla \rho\right), \tag{99}$$

by summing up the contribution of each three part we get the full conservation equation for the total energy,

$$\partial_t \left(\rho \hat{\mathcal{E}}\right) + \nabla \cdot \left(\rho \hat{\mathcal{E}} \hat{\boldsymbol{u}} + p \hat{\boldsymbol{u}} + \hat{\boldsymbol{\tau}} \cdot \hat{\boldsymbol{u}} + \boldsymbol{K} \cdot \hat{\boldsymbol{u}} + \kappa \rho \nabla \cdot \hat{\boldsymbol{u}} \nabla \rho + \boldsymbol{q}\right) = 0. \tag{100}$$

[1] N. Zhao, A. Mentrelli, T. Ruggeri, and M. Sugiyama, Physics of fluids **23**, 086101 (2011).
[2] A. Guardone and L. Vigevano, Journal of Computational Physics **175**, 50 (2002).
[3] P. Colonna and A. Guardone, Physics of Fluids **18**, 056101 (2006).
[4] D. Jamet, O. Lebaigue, N. Coutris, and J. Delhaye, Journal of Computational Physics **169**, 624 (2001).
[5] I. Polishuk, R. González, J. H. Vera, and H. Segura, Physical Chemistry Chemical Physics **6**, 5189 (2004).
[6] E. A. Guggenheim, The Journal of Chemical Physics **13**, 253 (1945).
[7] C. Zamfirescu, A. Guardone, and P. Colonna, Journal of Fluid Mechanics **599**, 363 (2008).
[8] B. J. Palmer and D. R. Rector, Physical Review E **61**, 5295 (2000).
[9] Q. Li, P. Zhou, and H. Yan, Physical Review E **94**, 043313 (2016).
[10] D. Lycett-Brown and K. H. Luo, Computers & Mathematics with Applications **67**, 350 (2014).
[11] A. Wagner, Physical Review E **74**, 056703 (2006).